Polymer 51 (2010) 3203–3212

Contents lists available at ScienceDirect

Polymer

journal homepage: www.elsevier.com/locate/polymer

Tensile tests in the environmental scanning electron microscope (ESEM) – Part I: Polypropylene homopolymers

P. Poelt [a,*], A. Zankel [a], M. Gahleitner [b], E. Ingolic [a], C. Grein [b]

[a] Institute for Electron Microscopy, Graz University of Technology, Steyrerg. 17, A-8010 Graz, Austria
[b] Borealis Polyolefine GmbH, St.-Peter Str. 25, A-4021 Linz, Austria

ARTICLE INFO

Article history:
Received 22 January 2010
Received in revised form
25 April 2010
Accepted 29 April 2010
Available online 11 May 2010

Keywords:
Tensile test
Polypropylene
Environmental scanning electron microscope

ABSTRACT

Performing tensile tests in an ESEM enables the simultaneous recording of both the force-elongation diagrams and the microstructures forming at the crack tip. Whereas the former are macroscopic parameters, the latter provide information on the micro-scale and are dependent both on the microstructure of the material itself and the test parameters. Changes in the fracture behaviour during a tensile test can be directly observed and correlated with the respective part of the force-elongation diagram.

Neat polypropylene samples with varying MFI values and different types of crystal modification and structure were investigated. Videos of the crack propagation at the crack tip clearly show that irreversible deformation already starts at forces far below the maximum load. The size of the spherulites seems to determine the size of the structures developing at the crack tip. Cyclic tests demonstrate that the respective structures can deform elastically, but they do not heal. Furthermore, relaxation experiments prove that relaxation does not take place at the central fracture region but beyond it. Decreasing the specimen temperature below the glass transition temperature of the material provides information about the change in the microstructures at the crack tip involved therewith.

1. Introduction

The elastic and plastic properties of polymers are strongly dependent on their microstructure. Some of the most important parameters for neat polypropylene are the volume fraction of the crystalline phase, the crystal modification distribution, the shape and size of the spherulites as well as the presence and amount of oriented crystalline superstructures [1–3]. Information about the elastic/plastic behaviour of polymers is generally obtained by tensile tests, bending tests and impact flexural tests. It should be noted, however, that both the characteristic curves recorded from these tests and the material constants deduced from them are global macroscopic parameters, integrated over all the microscopic processes taking place during the deformation or relaxation. A stress-strain characteristic, for example, does not give any immediate information on what is happening in the material on the micro-scale. In order to gain knowledge about the microstructures developing during these tests, investigations of cross sections prepared after the stop of the tests at a predetermined load or elongation are, therefore, generally made by light microscopy (LiMi), scanning electron (SEM) and transmission electron microscopy (TEM). But they provide only a snap-shot of the respective structures and many of these tests are necessary to shed light on the dynamic evolution of these microstructures during the test.

Performing tensile or bending tests in a SEM could be one possibility to overcome this shortcoming at least partly. Tests in the SEM enable the simultaneous recording of both the stress-strain diagram and the crack propagation, including the structures evolving at the crack tip. The latter can be recorded with high magnification and, still more important, great depth of focus either by video or by still images at predefined time intervals. The structures developing at the crack tip and their progression during the tensile test are strongly dependent on both the microstructure of the material itself and the test parameters, e.g. the test speed. As a consequence, correlations between the macroscopic characteristics and parameters and the microstructures formed at the crack tip during the test should be possible. These results should provide useful input both for the improvement of the theoretical models for the fracture behaviour of polymers and for the refinement of the respective simulation programs. The question might arise whether what is happening at the crack tip is really important for the

* Corresponding author. Tel.: +43 316 873 8321; fax: +43 316 811596.
E-mail address: peter.poelt@felmi-zfe.at (P. Poelt).

0032-3861/$ – see front matter © 2010 Elsevier Ltd. All rights reserved.
doi:10.1016/j.polymer.2010.04.068

Table 1
Basic data to the materials used in the investigation (mechanics and DSC data for non-nucleated versions of α-modification).

Polymer	MFI	ISO 527-2			
	230 °C/2.16 kg	Modulus	yield stress	ext. At yield	ext. At break
	g/10 min	Mpa	Mpa	%	%
PP-H1	0.3	1550	35.9	10.4	350
PP-H2	2.5	1580	35.5	9.2	370
PP-H3	20	1740	35.8	8.2	260

Polymer	Charpy ISO 179 1eA MWD (GPC)			DSC		
	NIS +23 °C	Mw	Mw/Mn	Tm	Hm	Tc
	kJ/m^2	kg/mol	–	°C	J/g	°C
PP-H1	7.2	980	6.6	164	105	112
PP-H2	4.3	570	6.6	165	107	116
PP-H3	2.1	300	5.7	166	112	121

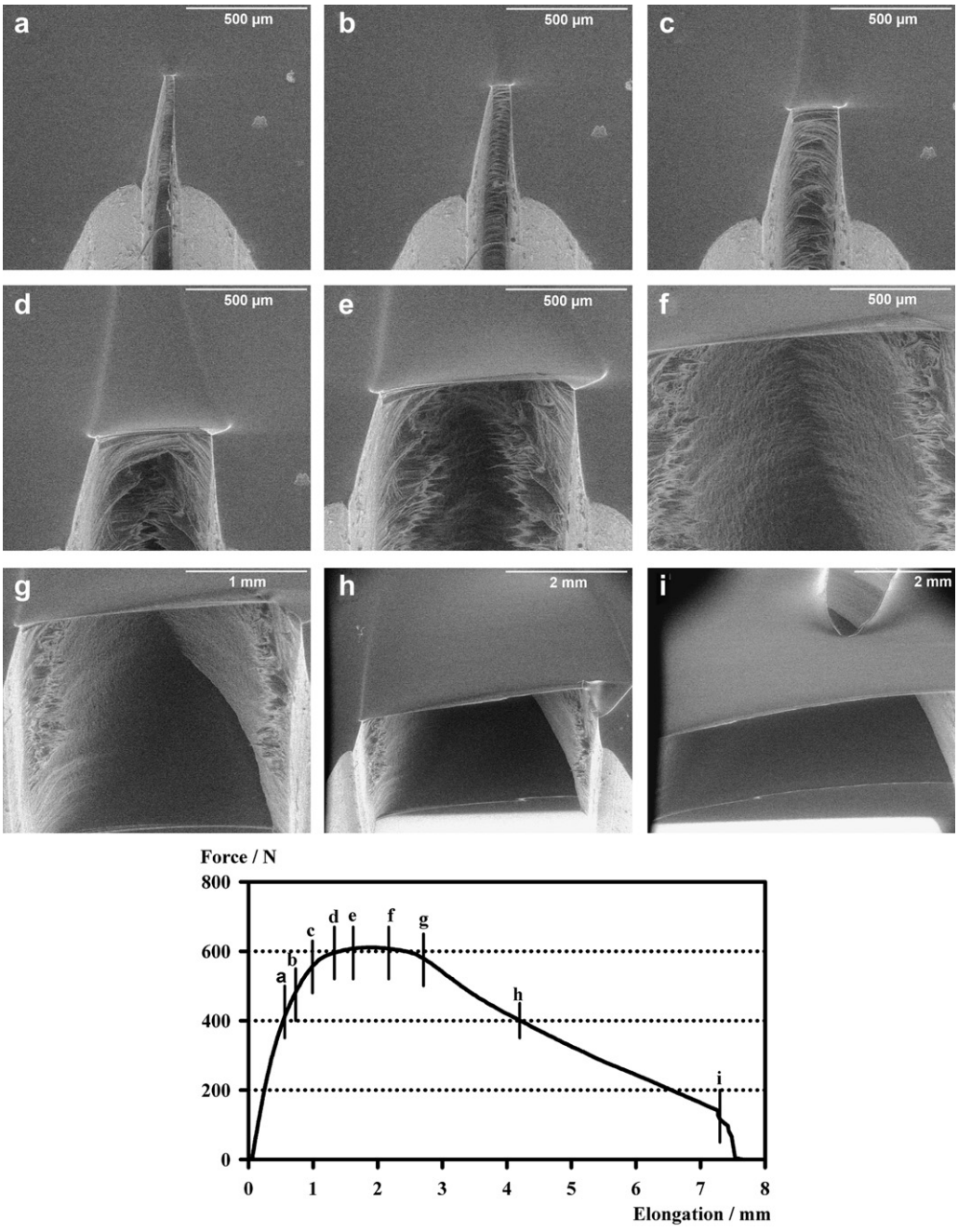

Fig. 1. Tensile test of iPP (MFI 20, β-nucleated), $v = 1$ mm/min. The images of the crack tip were recorded at the elongations marked in the force-elongation diagram below, with an increase in the elongation from image a to image i.

fracture of a bulk specimen. But for pre-cracked specimens initially strong stress concentration is taking place at the crack tip and thus at least for small strains most of the damage will occur there.

Such experiments were performed as early as 1976 by Smith et al. [4] and 1984 by Bandyopadhyay [5,6], but it seems they did not have a great impact on the interpretation of the fracture process of polymers. One reason may be that these experiments were performed in a conventional high vacuum SEM. In such an instrument, irradiation with electrons causes charging of the surface of uncoated electrically non-conductive specimens and therefore the images recorded become distorted unless a specific electron energy, normally close to 1 keV, is chosen for imaging. But imaging quality at such low energies was relatively poor in the early instruments. Furthermore, even in that case partial charging is often unavoidable, because the exact value of that electron energy is dependent on the type of material and can be different for the components of a polymer blend. To avoid charging, the specimens are generally coated with a thin conductive layer. But this is only possible as long as the uncoated new surface created is not too large. In-situ tensile tests in a conventional SEM were recently also performed by Zheng et al. [7] with modified polypropylene.

However, charging can also be avoided by use of an ESEM (Environmental Scanning Electron Microscope), which can be operated both in the high vacuum mode and in a vacuum range between 13 and around 1000 Pa. The positive gas ions formed by the scattering of the electrons at the gas atoms or molecules compensate the negative charge at the surface, enabling imaging at any electron energy.

Kim and Michler [8,9] investigated deformation processes of semi-thin polymer sections both in a high voltage TEM and a SEM. Investigations of thin sections in a SEM using a STEM detector were also carried out by Jornsanoh et al. [10]. No simultaneous recording of the stress-strain diagrams, however, was implemented in these experiments. But Nase et al. [11] performed in-situ peel tests in an ESEM and recorded videos of the tests as well as the force-elongation characteristics.

In the following sections it will be demonstrated that tensile tests in the ESEM can provide a wealth of information about the fracturing process of polymers. To gain the same results with the conventional methods would, if possible at all, be much more time-consuming.

2. Materials and methods

2.1. Materials

Three different PP homopolymers based on a commercial 4th generation Ziegler–Natta catalyst system including an organosilane donor and produced in a pilot unit using Borstar™ technology were supplied by Borealis Polyolefine GmbH (Linz, Austria) for this study (see Table 1 for polymer properties). Non-nucleated

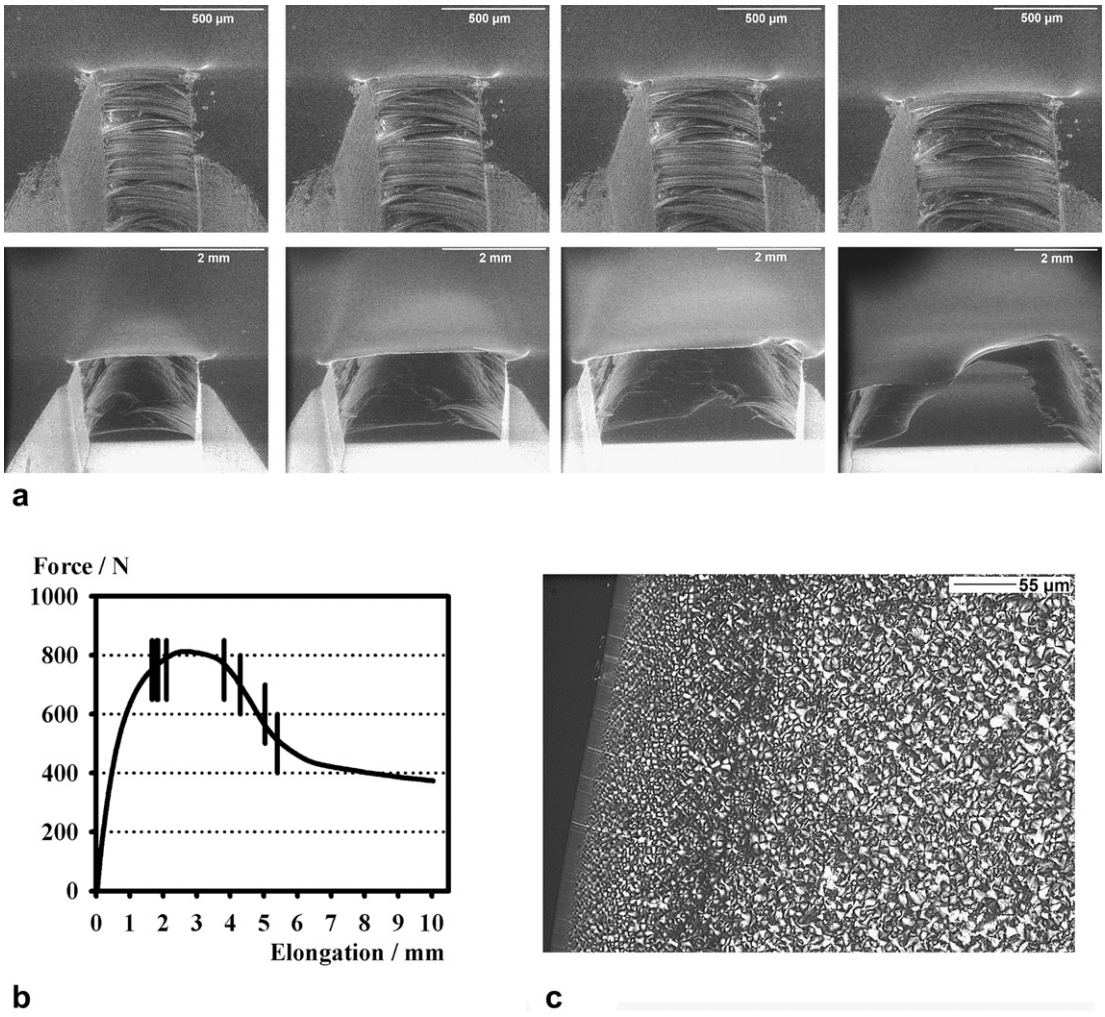

Fig. 2. Tensile test of iPP (MFI 2.5, non-nucleated), $v = 1$ mm/min; a: images of the crack tip recorded at the elongations marked in the force-elongation diagram in b, with an increase in the elongation from left to right and top to bottom. c: LiMi image of the skin of the specimen (thin section), with the bright spots indicating the spherulites.

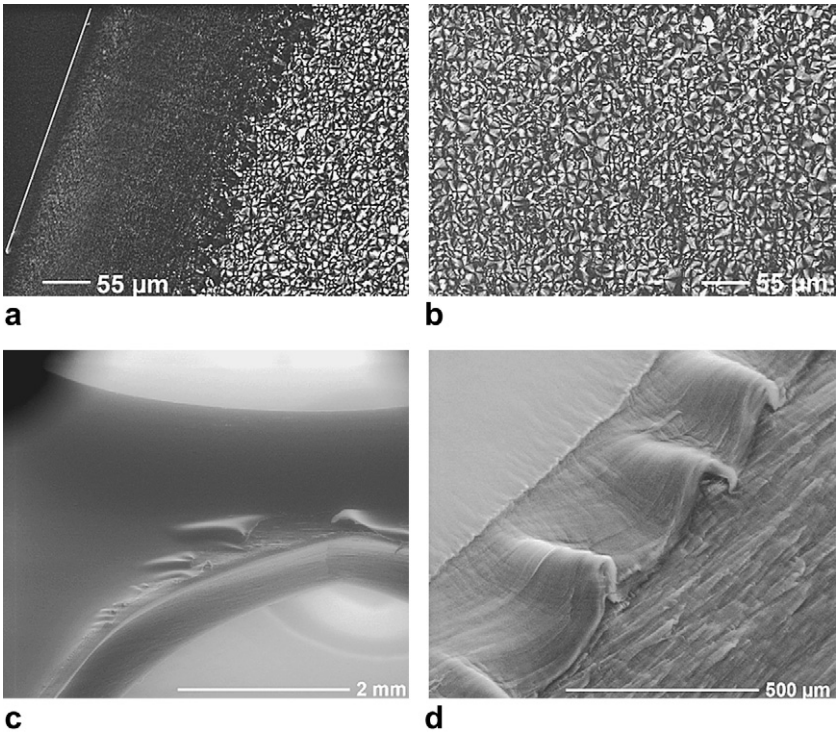

Fig. 3. iPP (MFI 20, β-nucleated); a, b: LiMi images of thin sections from the skin and the bulk of the specimen, with the bright spots indicating the spherulites. The white line in image a marks the surface. c, d: images showing the spalling of the skin during the tensile test.

and β-nucleated versions (using γ-quinacridone as nucleating agent, with a content of more than 80% of β-modification as determined by differential scanning calorimetry) of each material were tested on Charpy V-notch specimens of 80 × 10 × 4 mm^3 fabricated by injection molding.

The specimens were cut to sizes of 42/24 × 10 × 4 mm^3 for tensile tests performed at room/cryogenic temperature and differed in their viscosity and in the type and size of their spherulites. In addition to notching (depth: 2 mm), they were precracked (depth: 0.5 mm) with a razor blade immediately before the tensile test. Thus the actual cross-section at the fracture region was 7.5 × 4 mm. All materials were characterised before and after the tensile tests by light microscopy (LiMi), scanning (SEM) and transmission (TEM) electron microscopy.

2.2. Instrumentation

The tensile tests were carried out in an ESEM Quanta 600 FEG (FEI Eindhoven, NL) equipped with an MT5000 tensile stage (load cells: 5000 N, 1250 N and 125 N) of Deben (Suffolk, UK). The jaw velocity of the stage can be varied between 0.05 and 5 mm/min. Water vapour at a pressure of around 66 Pa was used as chamber gas. This amounts to a relative humidity of roughly 2.5%. Images and videos were generally recorded using an electron energy of 10 keV and a probe current of about 0.5 nA.

Tensile tests at temperatures below the glass transition temperature of polypropylene were performed using a modified heating/cooling platform from Gatan, Inc. (Pleasanton, CA, USA) with a temperature range between −100 °C and +200 °C [12]. To calibrate the actual temperature at the specimens for a given platform temperature, thermocouples were molded into the PP specimens to measure the specimen temperature for a series of predefined platform temperatures. A small temperature gradient across the 4 mm thick samples was unavoidable [12].

3. Results and discussion

3.1. The crack tip

Fig. 1 shows that at temperatures above the glass transition temperature and at the test speeds available, crack propagation always started with strong tip blunting, accompanied by the

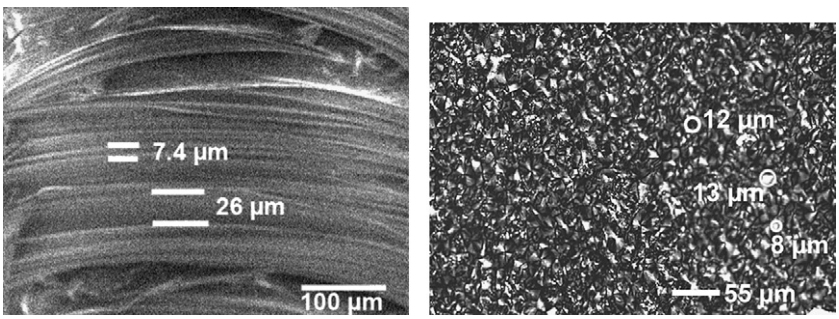

Fig. 4. iPP (MFI 2.5, non-nucleated); left: section of second image of top row of Fig. 2a; right: LiMi image of a thin section from the bulk of the specimen, with the bright spots indicating the spherulites.

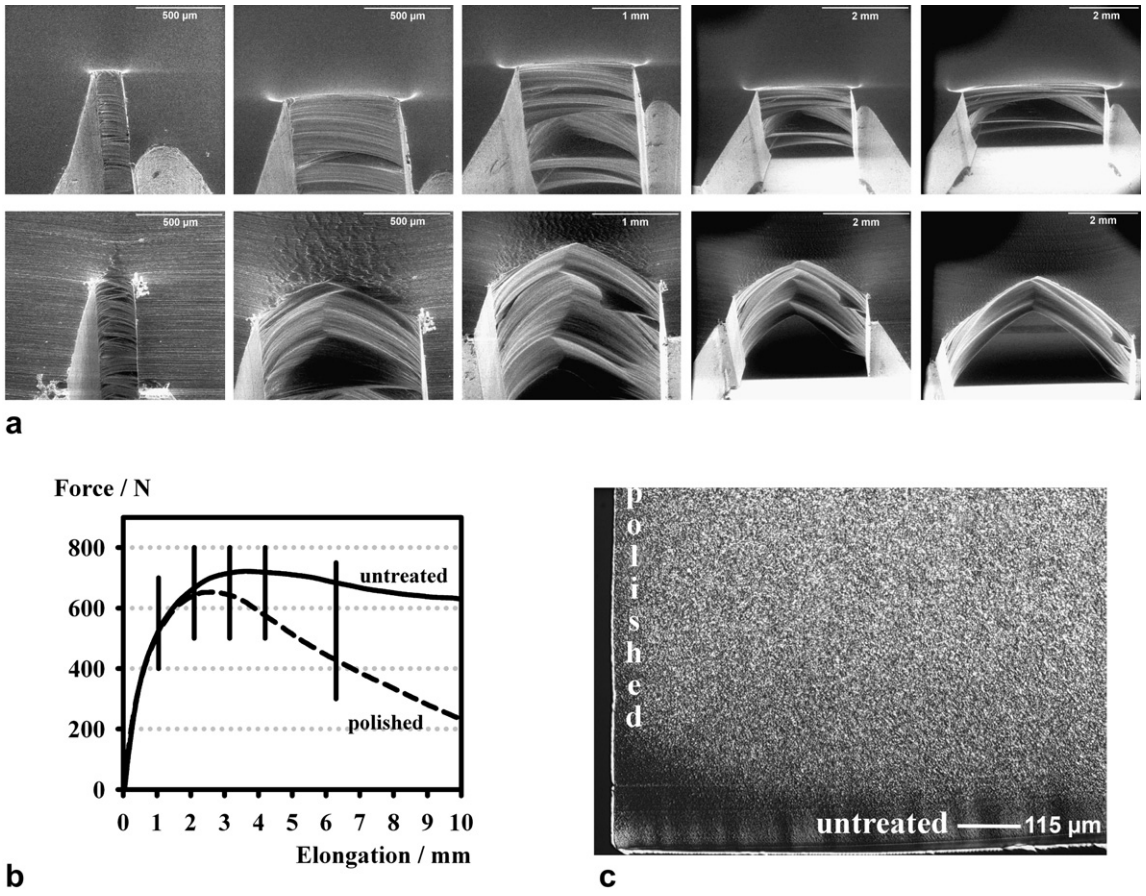

Fig. 5. Tensile test of iPP (MFI 2.5, β-nucleated), $v = 1$ mm/min; a: images of the crack tip recorded at the elongations marked in the force-elongation diagram in b, with an increase in the elongation from left to right. Top row: original specimen; bottom row: skin removed (0.2 mm). c: LiMi image of the skin of the specimen (thin section), partly polished.

formation of rather regularly arranged fibril-/craze-like structures at the crack tip [13,14]. To simplify matters, they will simply be called fibril-like structures in the following. It should be noted that the pressure in the specimen chamber of the microscope is much lower than ambient pressure. This could have an impact on the structures developing at the crack tip, for example the formation of small voids. To verify whether an influence of the pressure can be observed, a tensile test was started at ambient pressure and stopped at a force around half the maximum load.

Subsequently the specimen chamber was evacuated and the structures that had formed at the crack tip were imaged. These structures did not differ from those evolving at a similar test performed under full vacuum.

The evolution of the fibril-like structures during the tensile test can be clearly seen in the series of images in Fig. 1, showing the microstructures present at the crack tip at different elongations. These images were recorded during a tensile test of iPP (MFI 20, β-nucleated) with a test speed of 1 mm/min at the elongations marked in the corresponding force-elongation diagram. The exact nature of these structures is difficult to judge, because only their front surfaces are visible and it remains open whether cavities have already developed behind these structures. The images also demonstrate directly that inelastic deformation and damage at the crack tip occurs already at small forces far below the maximum load. Fig. 1 additionally reveals that the skin is much more ductile than the bulk. It seems that the fracturing of the skin does not start until the bulk is entirely fractured. The skin and the bulk will generally differ in their mechanical properties. But how strong these differences are will depend on the type of manufacture. Performing the tensile tests in the ESEM can give an immediate impression of this.

A comparison of the images d and f of Fig. 1 proves that during the tensile test a change in the fracture behaviour of the specimen takes place. Initially rather fierce rupturing of the fibril-like structures occurs, leaving pronounced shreds behind, as can be clearly seen in image e. Both the video recorded during the tensile test and the force-elongation diagram have a time axis, the latter simply by dividing the elongation by the test speed. Thus correlating the video with the respective force-elongation diagram proves that the transition takes place around the maximum load. This ductile fracture is then replaced by a rather semi-brittle fracture with much smoother fracture surfaces. This change in the fracture behaviour could also be seen from an image of the fracture surface recorded after the tensile test, but the video provides additional information at which force/elongation the transition in the fracture behaviour occurs. Brittle fracture in iPP (MFI 20) without β-spherulites occurred at the elongation at which ductile fracture started in the β-nucleated material.

A completely different fracture behaviour was observed for iPP (MFI 2.5). Around the maximum load tip blunting with fracturing of individual fibril-like structures occurred, but the crack tip scarcely advanced into the bulk (Fig. 2). Contrary to the tests of iPP (MFI 20), fierce fracturing occurred at the steeply declining part of the force-elongation diagram. Tensile tests in the ESEM thus immediately provide information about which type of fracture process takes place at different stages of the tensile test and how these processes relate to different parts of the force-elongation diagram.

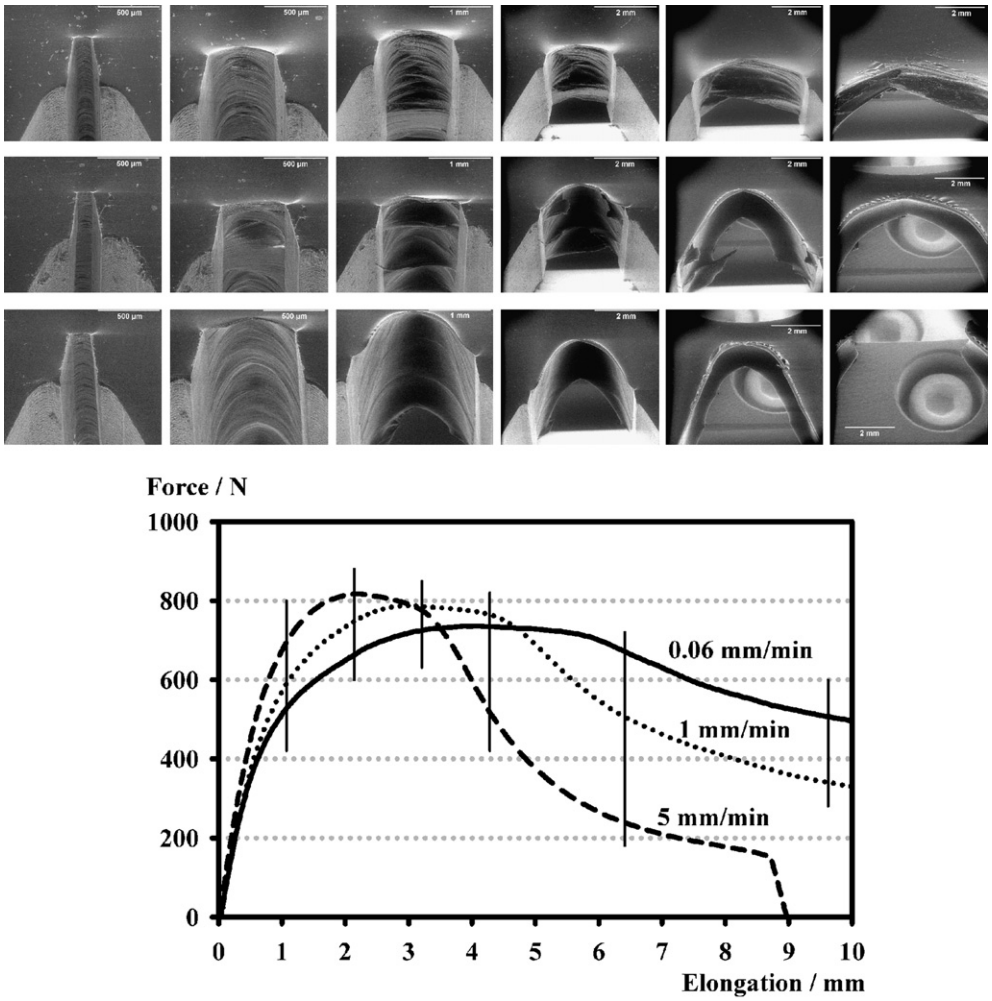

Fig. 6. Tensile test of iPP (MFI 0.3, non-nucleated), the three rows of images at the top were recorded at the elongations marked in the force-elongation diagram below, with an increase in the elongation from left to right. Top row: $v = 0.06$ mm/min, centre row: $v = 1$ mm/min; bottom row: $v = 5$ mm/min.

3.2. The skin

Figs. 1 and 2 demonstrate that in the samples used in the tensile tests the fracture of the skin started much later than that of the bulk. To investigate this phenomenon, thin sections were cut from the edge and the centre of the specimens. Images of these sections recorded by light microscopy indicate that the difference in the ductility of the skin and the bulk is most likely due to the different sizes and numbers of spherulites formed there (Fig. 2c). The skin was generally around 100 - 200 nm thick and often consisted of several layers. Similar images of iPP (MFI 0.3) can be seen in Fig. 3a and b, where also the formation of shear lips and a spalling of the skin can be observed at higher forces, with the individual layers becoming visible (Fig. 3d and e).

Possibly the formation and arrangement of the fibril-like structures visible at the crack tip in the early phase of the tensile tests are dependent on the size and distribution of the crystalline and amorphous phase in the material. Moreover, these structures seemed to form only if the size of the spherulites exceeded a specific threshold. Fig. 4 demonstrates that the width of the structures at the crack tip is comparable to that of the spherulites and that of the structures in between. Li et al. [15], in their investigation of the deformation mechanisms of β-polypropylene, argue that the orientation of the lamella of the spherulites with respect to the loading direction might be important for the formation of special deformation structures. For stresses below the yield stress,

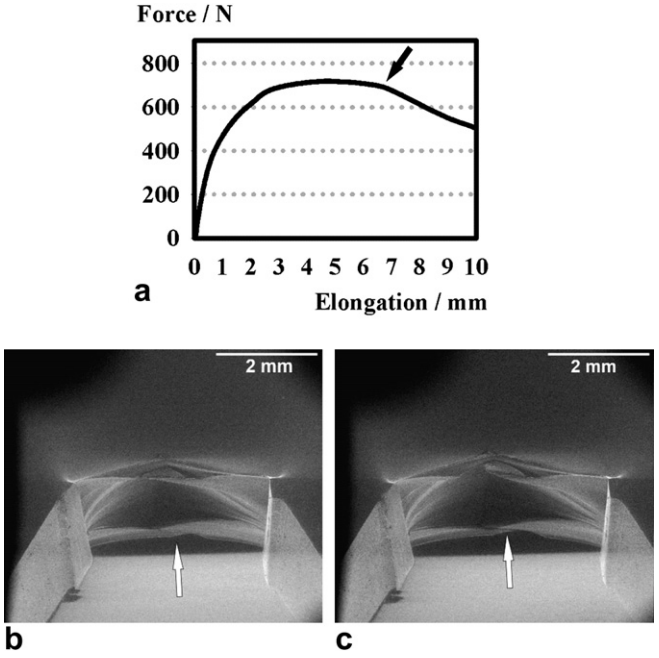

Fig. 7. Tensile test of iPP (MFI 0.3, β-nucleated), $v = 1$ mm/min; a: force-elongation diagram showing a kink, marked by an arrow; b, c: images recorded at elongations slightly below (b) and above (c) the elongation belonging to the kink.

however, those structures should be rather small and should not extend beyond the boundaries of the spherulites.

To shed light on the influence of the skin on the fracture behaviour of the bulk, the skin was removed by polishing. Fig. 5c proves that polishing did not damage the specimen substantially below the newly created surface. Tip blunting during the tensile tests is now stronger and the fibril-like structures disappear at lower elongations than for the specimens with the original skin in place (Fig. 5a). Thus, despite being very thin, the skin seems to keep the already fracturing bulk tightly together. But care must be taken in the interpretation of the results, because a 200 nm thick layer on each side of the specimen was removed by polishing, reducing the cross-section at the notch from $7.5 \times 4\,mm^2$ to around $7.1 \times 3.6\,mm^2$. Thus at least part of the difference in the force-elongation diagrams presented in Fig. 5b is due to the difference in the cross-sections of the specimens.

3.3. The test speed

The evolution of the structures at the crack tip is not only dependent on the microstructure of the material, but also on the test parameters. Fig. 6 demonstrates that with increasing test speeds both a well-defined tip blunting and the fibril-like structures disappear at decreasing elongations. Thus, one can suppose the existence of a critical test speed above which these structures no longer appear, not even immediately after the start of the tensile test. Possibly this critical speed is linked with the relaxation time constants of the respective material, because they determine how quickly the molecules of the polymer can rearrange themselves. This critical speed may also be linked with the speed at which a transition from a ductile to brittle fracture behaviour can be observed [16].

The structures of β-nucleated iPP evolving at the crack tip resemble those of iPP with α-spherulites only. But due to the more ductile behaviour of the β-spherulites compared to α-spherulites [16,17], the overall behaviour at the crack tip corresponds to that of α-PP tested with a lower test speed.

A kink is visible in the force-elongation diagram of iPP (MFI 0.3, β-nucleated) recorded at a test speed of 1 mm/min (see arrow in Fig. 7a). The progress in the fracture process as illustrated in the Fig. 7b and c seems to indicate that this kink is due to the sudden rupture of a bigger structure, possibly a whole bundle of fibres,

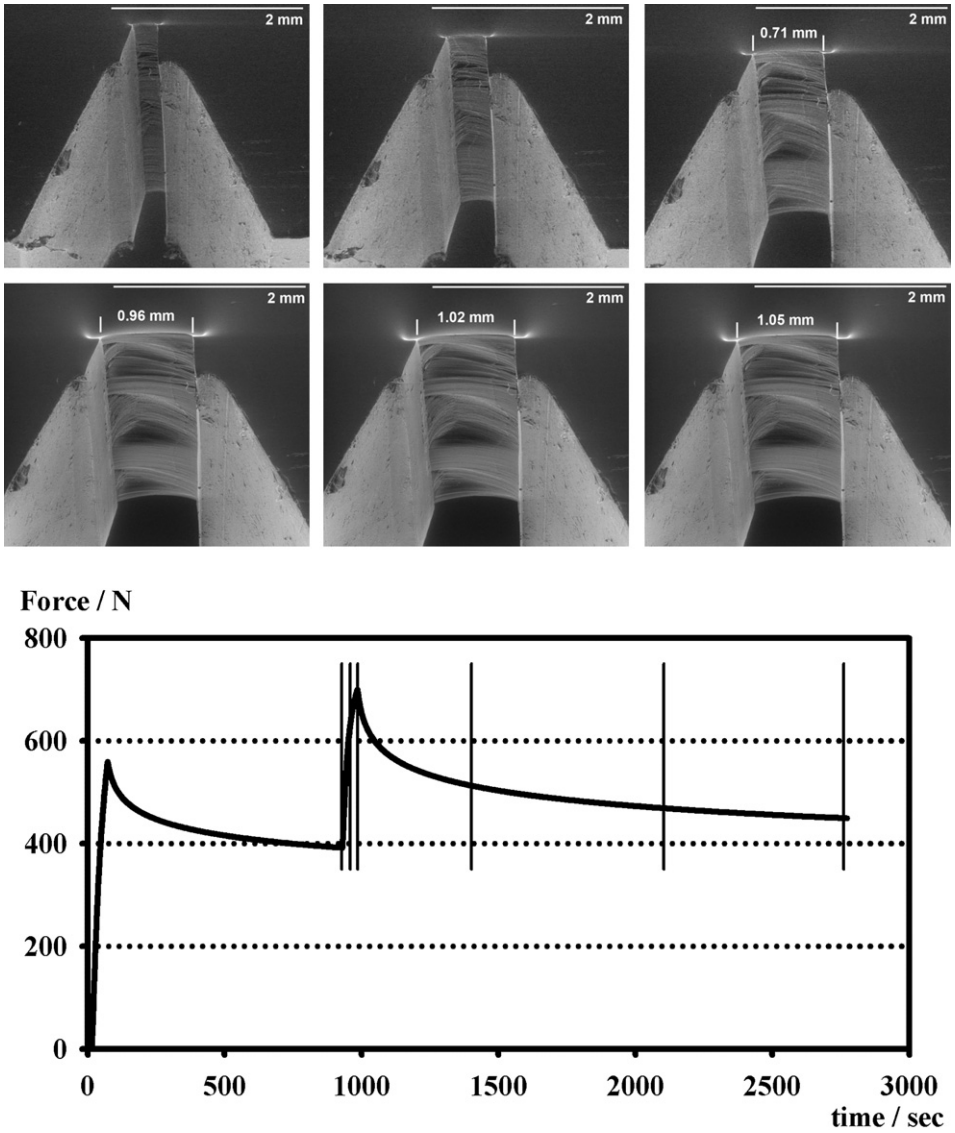

Fig. 8. Tensile test with subsequent relaxation of iPP (MFI 2.5, β-nucleated), $v = 1$ mm/min. The images of the crack tip were recorded at the elongations marked in the force-elongation diagram below, with an increase in the elongation from left to right and top to bottom.

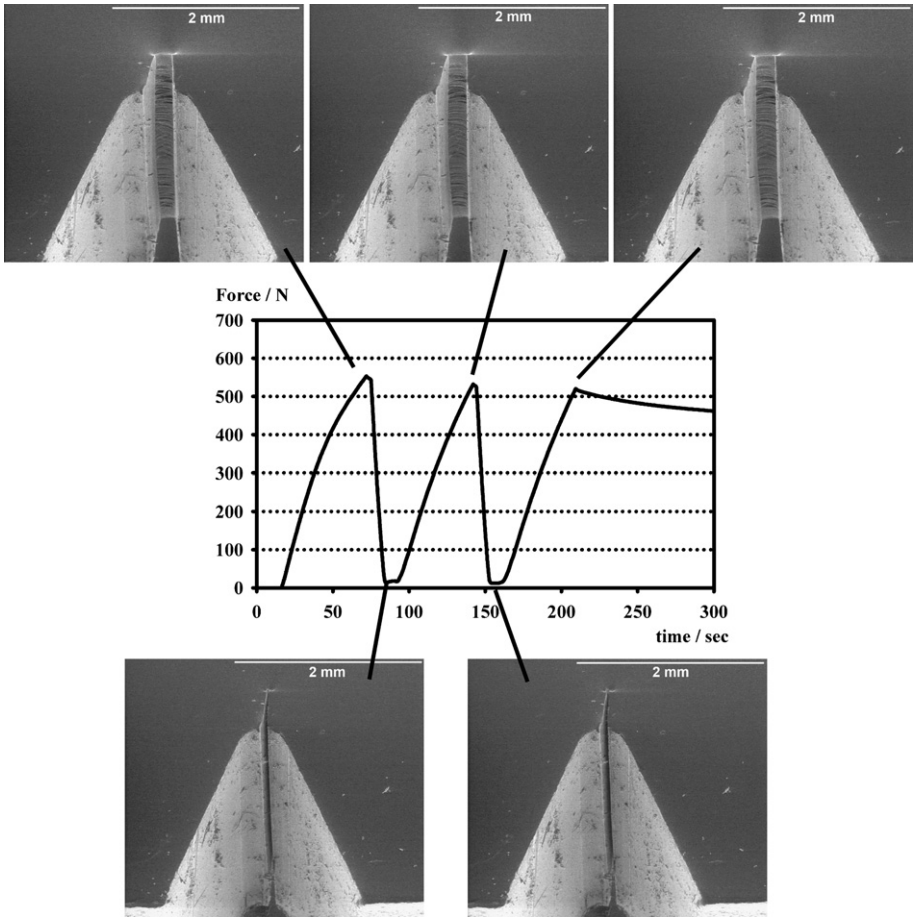

Fig. 9. Cyclic test of iPP (MFI 2.5, β-nucleated), up: $v = 1$ mm/min, down: $v = 5$ mm/min.

marked by an arrow in both figures. This would also prove that the processes occurring at the crack tip are definitely not negligible compared to those going on in the bulk and contribute substantially to the progression of the force-elongation characteristic. Thus, the smooth gradient of the stress-strain diagram should, at least in part, be due to the successive fracture of individual fibril-like structures. As these structures are not formed at high test speeds, such phenomena will not occur at those speeds. As a consequence, the fracture mechanisms below and above the critical speed may be of a completely different type. A ductile–brittle transition with increasing test speed was for example reported by Gensler et al. [18].

3.4. Relaxation and cyclic tests

Plastic deformation and damage of PP in the fracture region starts at rather low stresses, far below the maximum load. This can also be proven by other experiments like x-ray densitometry.

Complete recovery during relaxation is, of course, not possible for deformations extending the elastic range. But the series of images in Fig. 8 demonstrates that during relaxation inelastic deformation still increases at the central fracture region. The front face of the fracture zone still widens substantially, from around 0.71 mm to 1.05 mm during the first 30 min of relaxation. In fact, relaxation will occur mainly outside the fracture zone, where elastic deformation still prevails. In this area the elastic deformation relaxes, thus reducing this part of the specimen in length. Since the entire length of the stretched specimen needs to be constant, the central fracture zone is still pulled apart during the relaxation process. This compensation causes the damage to progress. This may be different for other polymers experiencing relaxation at the same elongation and in the case of PP is due to the fact that irreversible deformation and damage occur already at forces far below the maximum load.

To calculate the relaxation time constants, an equation with two exponentials was used, corresponding to the Maxwell model [19]. The time constants were $t_1 = 39$ s and $t_2 = 385$ s for a strain $\varepsilon = 0.025$ (the first relaxation in Fig. 8) and $t_1 = 61$ s and $t_2 = 714$ s for $\varepsilon = 0.05$ (the second relaxation in Fig. 8).

The cyclic test in Fig. 9 shows a nearly exact replication of the tip blunting and especially also an exact reproduction of the structures at the crack tip during the successive cycles, as long as the force is not increased above that of the previous cycle. Thus no substantial modification of the deformed structures and no real recovery seem to occur when returning to force zero, at least not at the crack tip. Otherwise such a perfect replication of the deformation structures could not be expected.

The images in Fig. 10, recorded at the same force but with a change in the direction of the force, the force in the cyclic test going both up and down, show that the fibril-like structures look the same independent of the direction of the force, i.e. whether the force is increasing or decreasing. Thus these structures themselves seem to deform elastically during the cyclic tests. But no healing of the damaged structure takes place. Healing can only be expected for very small structures, like voids with diameters smaller than 20 nm, whereas bigger ones remain stable [20]. The original state is

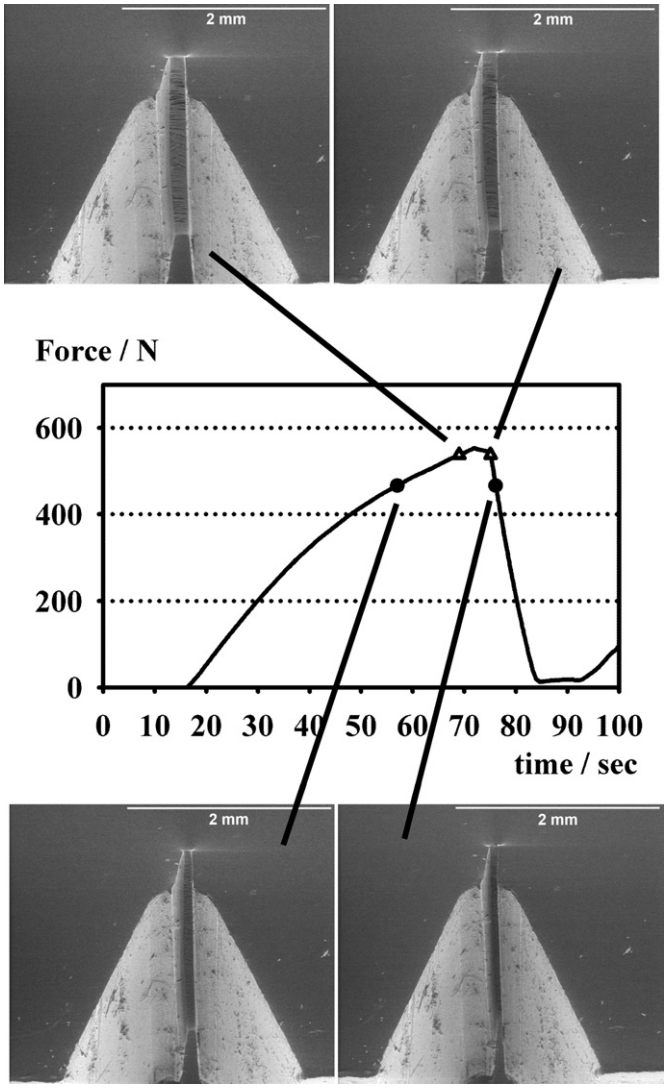

Fig. 10. Cyclic test of iPP (MFI 2.5, β-nucleated), up: $v = 1$ mm/min, down: $v = 5$ mm/min.

only restored in the elastically strained regions outside the fracture zone.

3.5. Below the glass transition temperature

Below the glass transition temperature T_g polymers become brittle. The force-elongation diagrams in Fig. 11 demonstrate that the respective diagrams for iPP with a MFI 0.3 at around −64 °C and iPP with a MFI 20 at room temperature have a very similar shape. This is not surprising, because both going below T_g and enhancing the MFI index enhances the brittleness. Thus the question arises of whether the fracture mechanisms are the same in both cases. But a comparison of these two cases may be doubtful because of the large difference in tensile strength.

As can be seen from the images in Fig. 11, tip blunting and advance of the crack tip into the material occurs, similar to the tensile tests at room temperature. But the typical fibril-like structures are no longer visible, the region at the crack tip looks rather smooth. Structures at the crack tip begin to appear only at elongations close to the value where fracturing occurs. But they are very irregular, include the formation of cavities and do not really resemble the fibril-like structures dominating at room temperature at comparable elongations. This may be explained by the fact that below T_g the amorphous material has become brittle, lost its ability to deform elastically or plastically and that therefore the properties of the amorphous and crystalline parts of the polymer converge.

A temperature rise in the fracture region should not occur at these test speeds and thus the actual temperature at the crack tip should be that measured at the bulk. Van der Wal and Gaymans [21] showed for PP rubber blends that a temperature rise is only observed at velocities exceeding approximately 5–10 m/s, which is far beyond the test speeds used in this work.

4. Conclusion

The great advantage of tensile tests in an ESEM is the additional information available from high resolution images of the crack tip, which are simultaneously recorded with the force-elongation diagrams. The microstructures forming there and their evolution during the tensile test are dependent both on the microstructure of the material itself and on the test parameters chosen for the tensile test.

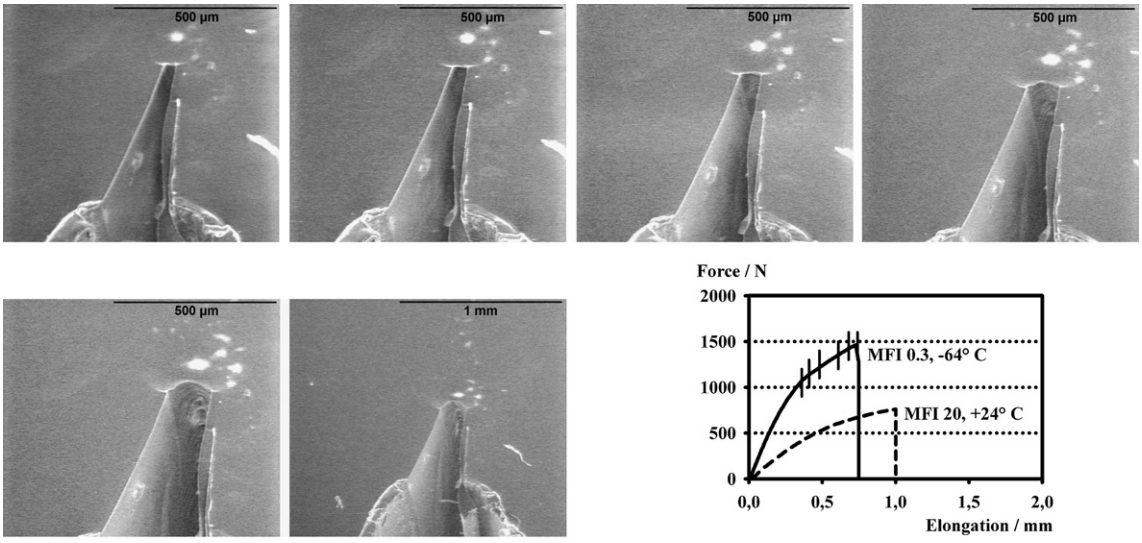

Fig. 11. Tensile tests of iPP (MFI 20, non-nucleated) at $T = 24$ °C and iPP (MFI 0.3) at $T = -64$ °C, $v = 1$ mm/min. The images of the crack tip (test at $T = -64$ °C) were recorded at the elongations marked in the force-elongation diagram, with an increase in the elongation from left to right and top to bottom.

Tensile tests were performed with neat polypropylene specimens varying in their MFI and the type of crystal modification (non-nucleated in α-form and β-nucleated). The parameters test speed and specimen temperature were varied during the tests. In most cases the formation of fibril-/craze-like structures was observed at the crack tip. But if the size of the spherulites falls below a certain limit or the test speed exceeds a specific value, these structures no longer appear. The same is true if the specimen temperature is far below the glass transition temperature of the polymer. Relationships between the force-elongation diagram and the evolution of microstructures at the crack tip can be established.

Relaxation and cyclic tests were performed at elongations beyond the elastic range. It is clearly visible, that in these cases relaxation does not occur in the central fracture region, but outside the fracture zone, where elastic deformation still prevails. By contrast, in the central fracture region damage still progresses during the relaxation process. Additionally, cyclic tests show that the structures forming at the crack tip can deform elastically, but no healing takes place.

Acknowledgements

This work was sponsored by the Austrian Research Promotion Agency (Project: 809.817).

References

[1] Eder G, Janeschitz-Kriegl H. Structure development during processing. 5. Crystallization. Materials and technology series. Weinheim: Verlag Chemie-Wiley; 1997. 269–342.
[2] Phillips R, Herbert G, News J, Wolkowicz M. Polym Eng Sci 1994;34:1731–43.
[3] Gahleitner M, Wolfschwenger J, Bernreitner K, Neißl W, Bachner C. J Appl Polym Sci 1996;61:649–56.
[4] Smith K, Hall MG, Hay JN. J Polym Sci Polym Lett Ed 1976;14:751–5.
[5] Bandyopadhyay S. J Mat Sci Lett 1984;3:39–43.
[6] Bandyopadhyay S, Silva VM. Proc 6th Intern Conf on Fracture – ICF6, 4. Pergamon Press; 1984. 2971–2978.
[7] Zheng Y, Shen Z, Wang M, Ma S, Xing Y. J Appl. Polym Sci 2007;106:3736–42.
[8] Kim G-M, Michler GH. J Appl Polym Sci 1996;60:1391–403.
[9] Kim G-M, Michler GH. Polymer 1998;39:5689–97.
[10] Jornsanoh P, Thollet G, Gauthier C, Massenelli-Varlot. In: Richter S, Schwedt A, editors. Proc EMC 2008, 2. Springer; 2008. p. 771–2.
[11] Nase M, Zankel A, Langer B, Baumann HJ, Grellmann W, Poelt P. Polymer 2008;49:5458–66.
[12] Zankel A, Poelt P, Gahleitner M, Ingolic E, Grein C. Scanning 2007;29:261–9.
[13] Poelt P, Zankel A, Gahleitner M, Grein C, Ingolic E. Proc DYFP 13. Kerkrade; 2006. 331–334.
[14] Poelt P, Zankel A, Gahleitner M, Herbst H, Ingolic E, Grein C. Proc PPS 24 (CD). Salerno; 2008. 1–5.
[15] Li JX, Cheung WL, Chan CM. Polymer 1999;40:2089–102.
[16] Grein C, Plummer CJG, Kausch H-H, Germain Y, Béguelin Ph. Polymer 2002;43:3279–93.
[17] Aboulfaraj M, G'Sell C, Ulrich B, Dahoun A. Polymer 1995;36:731–42.
[18] Gensler R, Plummer CJG, Grein C, Kausch H- H. Polymer 2000;41:3809–19.
[19] Menges G, Haberstroh E, Michaeli W, Schmachtenberg E. Werkstoffkunde Kunststoffe. 5th ed. München, Wien: Hanser; 2002. 105.
[20] Pawlak A, Galeski A. Macromolec 2005;38:9688–97.
[21] Van der Wal A, Gaymans RJ. Polymer 1999;40:6045–55.